The $^2/_3$ Power Law Dependence of Capillary Force on Normal Load in Nanoscopic Friction

E. Riedo,*,†,§ I. Palaci,† C. Boragno,‡ and H. Brune†

Institut de Physique des Nanostructures, Ecole Polytechnique Fédérale de Lausanne (EPFL), CH-1015 Lausanne, Switzerland, School of Physics, Georgia Institute of Technology, 837 State Street, Atlanta, Georgia 30332, and Universitá di Genova, Italy

Received: July 16, 2003; In Final Form: February 20, 2004

During the sliding of an atomic force microscope (AFM) tip on a rough hydrophilic surface, water capillary bridges form between the tip and the asperities of the sample surface. These water bridges give rise to capillary and friction forces. We show that the capillary force increases with the normal load following a $^2/_3$ power law. We trace back this behavior to the load induced change of the tip−surface contact area which determines the number of asperities where the bridges can form. An analytical relationship is derived which fully explains the observed interplay between humidity, velocity, and normal load in nanoscopic friction.

Introduction

The capillary force between two surfaces due to the formation of a liquid meniscus plays a central role in many physical, chemical, and biological phenomena.[1] From a technological point of view, the reliability of hard disks, aerospace components, and miniature motors depends on the ability to control surface forces such as friction and capillary forces at the microdown to the nanoscale.[2,3] Atomic force microscopy (AFM) has become a powerful technique to study surface forces at the nanoscale,[4−8] and the AFM tip sliding on a surface can often be considered as a model system for technologically relevant devices.

The quantitative study of capillarity can be traced back to the 19th century and has its root in the work of Young, Laplace, and Kelvin.[9] For a long time a very simple equation deduced from their theories has been used to describe the capillary force, F_c, between an ideally smooth spherical tip of radius R_T and a flat surface:[1,10−12]

$$F_c = 2\pi R_T \gamma(\cos\theta_T + \cos\theta_S) \qquad (1)$$

where γ is the liquid tension and θ_T and θ_S are the contact angles of the tip and the flat surface, respectively. However, several discrepancies have been found between experiments and eq 1. First, in eq 1 F_c is humidity independent whereas F_c was observed to increase with increasing humidity.[7,13−16] Furthermore, eq 1 applies only at equilibrium stationary conditions, that is, when the tip and the surface stay in contact for a sufficiently long time. If the contact time is below a critical value, it has been observed that F_c increases with increasing contact times.[16,17] Another assumption in eq 1 is that the surfaces in contact are perfectly smooth, and of course this is not always the case for real surfaces. Recent investigations have demonstrated that the surface roughness plays a crucial role in the humidity and time dependence of capillary forces.[16−19] These studies show that many capillaries can form between the asperities of two surfaces in contact, and this leads to an increase of F_c with increasing contact time and humidity. Finally, in eq 1 F_c does not depend on the normal load, whereas recent studies have shown that for rough surfaces the adhesion forces can depend on the normal load if there are plastic deformations of the asperities in the contact.[20,21] The normal load dependence of the capillary force for multiasperity contacts in the elastic regime has important consequences on the macroscopic properties of granular materials as well as in nanoscopic devices. Despite this, it has not been studied so far.

In this paper we show that the capillary force between a spherical AFM tip and a rough flat surface increases with the normal load, F_N, following a $^2/_3$ power law. This behavior is traced back to the fact that the number of asperities where the capillary bridges can form is proportional to $F_N^{2/3}$. In the following, we first measure the capillary force between an AFM tip and a glass surface through sliding friction force versus load measurements at different humidities and velocities. We show that these experiments can be explained only with a 0.7 ± 0.1 power law dependence of the capillary force on the normal load. Second, we develop a model for the load dependent capillary force which fully reproduces the experimental load dependence of the friction force over the investigated range of velocities and humidities.

Lord Kelvin was the first to derive the following relationship between the equilibrium vapor pressure of a liquid, P, and the mean radius of curvature, r_K, of the liquid/vapor interface:[1,11]

$$\frac{1}{r_K} = \frac{k_B T}{\gamma V_M} \ln\left(\frac{P}{P_S}\right) \qquad (2)$$

where V_M is the molecular volume of the liquid and P_S the saturated vapor pressure. This equation has been proven to be valid down to a few nanometers.[11] Under ambient conditions r_K is about 1 nm,[1] and as a consequence, water bridges are able to condense in nanometer-scale interstices. However, it may take a long time to reach the equilibrium state, since the formation of a water bridge is a thermally activated process.[16,17,20] The energy barrier for the formation of bridges of height h and cross section R_c^2 is $\Delta E(h) = k_B T \ln(P_S/P) h R_c^2/V_M$. By considering the thermally activated capillary condensation between two rough surfaces sliding one on the other, two important effects have been observed.[16] First, for longer contact times (lower sliding velocities) bridges can form also between more distant asperities. Since the distribution of the asperity distances is broad, the number of formed capillaries, N_c, increases with

† Ecole Polytechnique Fédérale de Lausanne (EPFL).
§ Georgia Institute of Technology.
‡ Universitá di Genova.

10.1021/jp0360624 CCC: $27.50
Published on Web 04/01/2004

decreasing sliding velocities. Second, since ΔE decreases with increasing humidity, N_c also increases with the relative humidity. The velocity and humidity dependence of N_c can be calculated analytically following the steps reported in ref 16 to yield

$$N_c = \begin{bmatrix} \left(\frac{V_M}{\lambda R_c^2}\right) \frac{\ln \frac{v_0}{v}}{\ln \frac{P_S}{P}} N_c^{tot} & : & v_{min} < v < v_0, P < P_{max} \\ 0 & : & v \geq v_0 \\ 1 & : & v \leq v_{min}, P \geq P_{max} \end{bmatrix} \quad (3)$$

where λ is the full width at half-maximum of the interstitial height distribution,[17] v_0, v_{min}, and P_{max} are critical parameters, and N_c^{tot} is the total number of asperities where the capillaries can form. Once N_c is calculated, we can deduce the total capillary force as the capillary force acting on each asperity times N_c:

$$F_c \cong 2\pi\gamma R_a(\cos\theta_T + \cos\theta_S)N_c \quad (4)$$

where N_c is given by eq 3 and R_a is the average radius of the asperities. This equation shows how the capillary force increases with the humidity and decreases with the logarithm of the sliding velocity in agreement with the experiments reported in ref 16 on CrN thin films. However, in ref 16 the role of the normal load on the capillary force has not been investigated, while here we concentrate on the study of the load dependence of the capillary force.

Experimental Section

Our experiments were performed on a standard glass sheet with a root-mean-square, rms, roughness of 1 nm on a 1 μm^2 surface. The capillary force has been investigated through friction force, F_F, measurements at room temperature by means of an AFM (AutoProbe M5). For humidity control, the AFM was placed in a tight box with inlets for dry and water-saturated nitrogen. We used V-shaped silicon cantilevers (Ultralevers type B) with normal and lateral spring constants of 0.4 and 50 N/m, respectively, and silicon conical tips with a nominal radius of curvature greater than 10 nm. The normal and friction forces are proportional to the normal and the lateral deflections of the cantilever which are recorded simultaneously. We define $F_N = 0$ nN at the point where the cantilever is not bent. Relative changes of the lateral forces were determined accurately by using the same cantilever throughout a series of experiments. The velocity dependence of friction was investigated in varying the scan frequency at fixed size. We verified that different scan sizes at constant frequency yielded consistent results. All the measurements at different loads were reversible; this means that we were always in the elastic regime.

Results and Discussion

Figure 1a shows the friction force as a function of the normal load at different sliding velocities for a fixed humidity $P/P_S = 0.33$. In Figure 1b F_F is plotted as a function of ln v at $F_N = 2$, 6, and 10 nN. First of all, we observe that F_F increases with the normal load following a power law with an exponent significantly lower than 1. This is in agreement with previous AFM experiments which found[3,22,23,27]

$$F_F \cong \mu_0(F_N + F_{adh})^{2/3} \quad (5)$$

where μ_0 is a parameter with a meaning similar to the friction coefficient and F_{adh} is the adhesion force which is mainly composed of van der Waals solid−solid forces and capillary forces.[13,24] Since in the elastic regime the friction force is proportional to the contact area,[25] the power law dependence of the friction force on the normal load can be traced back to the load dependence of the contact area. Different models have been developed to study this dependence in the case of single- and multiasperity contacts[26−29] and self-affine surfaces.[30] For the first case a $^2/_3$ power law dependence is usually found, whereas for the last two cases a linear dependence is more likely. Of course the border between a single- and a multiasperity contact is difficult to define, and it is unclear whether continuum contact mechanics is still valid at the nanoscopic scale. Nevertheless, following these lines of thought, if the primary result of increasing the load is to cause existing contacts to grow and not to form new contacts inside the apparent contact area, we still are in the single-asperity regime and F_F will not increase linearly with F_N.[3]

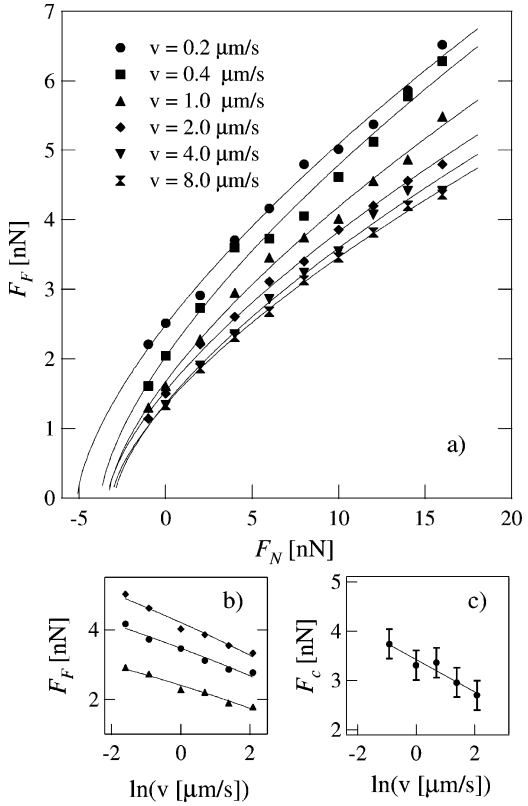

Figure 1. (a) Friction force vs normal load for different sliding velocities at a relative humidity of 33%. The solid lines are fits using eq 6. (b) The same data at $F_N = 2$, 6, and 10 nN from the bottom to the top, respectively, but F_F is now plotted as a function of ln v. (c) F_c, i.e., the value of F_N when $F_F = 0$, as a function of ln v.

According to eq 5, the value of F_N when $F_F = 0$ in Figure 1a is the adhesion force. Since in our experiments the capillary forces are much greater than all the other adhesive forces, that is, at low humidity ($P/P_S = 0.5$) the adhesive force is lower than 1 nN,[13,24] we can write $F_{adh} \simeq F_c$. Parts b and c of Figure 1 show that F_F and F_c decrease with ln v. The same behavior for F_F at three different humidities is reported in Figure 2. This figure shows that the slope of the F_F versus ln v curves decreases with decreasing humidity and is almost zero at very low humidities. We point out that on the same glass surface at even lower humidities and in ultrahigh vacuum or on an atomically flat mica surface in air, the friction increases with the velocity because of a thermally activated stick and slip process.[31] All

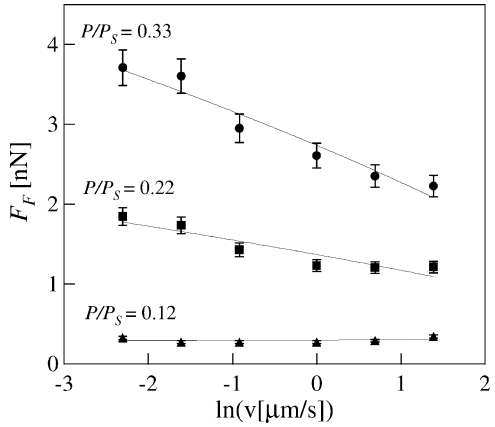

Figure 2. Friction force as a function of ln v for three different humidities, at $F_N = 4$ nN. The solid lines are fits with the relationship $F_F = (A - B \ln v)^{2/3}$, with A and B free-fitting parameters.

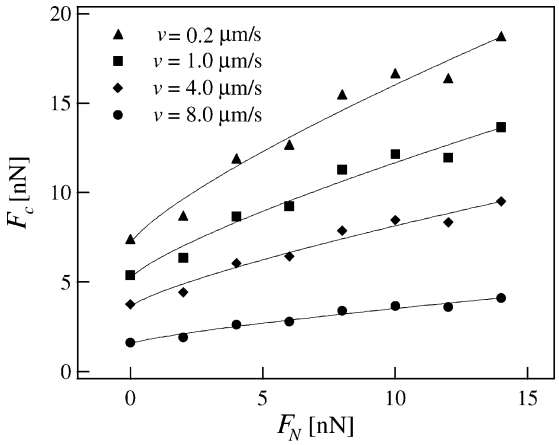

Figure 3. Capillary force as a function of normal load at different velocities. The solid lines are fits with the relationship $F_c = (A + BF_N)^{2/3}$, with A and B free-fitting parameters.

these results are in perfect agreement with the study in ref 16 and with eqs 3 and 4 through eq 5. According to these findings and the above equations we write

$$F_F \cong \mu_0(F_N + F_c)^{2/3} \cong \mu_0\left(F_N + f_c \ln\frac{v_0}{v}\right)^{2/3} \qquad (6)$$

where f_c is a function of the humidity. Moreover, we note that the velocity and load dependence of friction shown in Figure 1 put in evidence that the slope of the F_F versus F_N curves increases by decreasing the velocity, that is, the slope of the F_F versus ln v curves increases with increasing loads. This means that by increasing the sliding velocity we have not only a shift of the curves on the F_N-axis due to a decrease of F_c according to eq 4, but also a decrease of the slope. This effect can be explained with the increase of f_c with increasing loads. The data in Figure 1a can be plotted by using as independent variable, ln v. F_F versus ln v data at different loads have been fitted with $F_F = \mu_0(F_N + f_c \ln(v_0/v))^{2/3}$. From this fitting procedure we find the values of $\mu_0 f_c$ at different loads. By solving the equations for the intercepts at different loads, we also obtain the value of ln v_0 and μ_0. The capillary force $F_c = f_c \ln(v_0/v)$ is then plotted as a function of the normal load at different velocities as shown in Figure 3. The resulting power law of the capillary force on F_N is 0.7 ± 0.1.

The normal load dependence of F_c is hidden in eq 3 in the term N_c^{tot} via the number of asperities close enough to permit

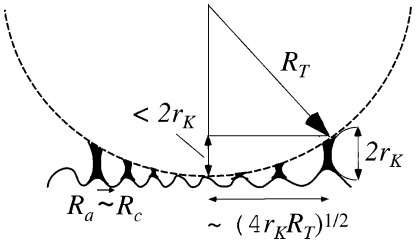

Figure 4. Capillary water bridges in the contact area between the AFM tip and the sample. We show the tip, capillary, asperity, and Kelvin radii. Since $R_T \gg r_K$, the radius which defines the area where the capillary can form, i.e., when the tip and the sample are closer than $2r_K$, is about $(4r_K R_T)^{1/2}$.

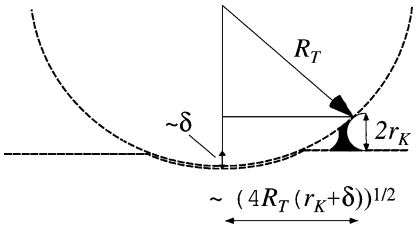

Figure 5. The new radius $(4R_T(r_K + \delta))^{1/2}$ which defines the area where the capillary can form when the tip penetrates the surface for a depth δ.

capillary condensation. As found by Kelvin, water condenses in interstices which are smaller than $2r_K$. This means that the available surface where the capillaries can form is $A_{av} \approx 4\pi r_K R_T$ (see Figure 4). N_c^{tot} can be written as the ratio between A_{av} and the area of one capillary πR_c^2. R_c has an intermediate value between r_K and R_a; however, the surfaces investigated in this experiment have $R_a \approx 1$ nm, and thus, at ambient conditions $r_K \approx R_a \approx R_c$. The deformation of the tip and the surface once in contact can be taken into account by writing, from geometrical considerations (see Figure 5), $A_{av} \approx 4\pi r_K R_T(1 + \delta/r_K)$, where δ is the indentation depth. Using the Hertz theory to estimate δ,[26] we can write $A_{av} \approx 4\pi r_K R_T(1 + KF_N^{2/3})$ where

$$K = \frac{1}{r_K}\left(\frac{9}{16R_T E^2}\right)^{1/3} \qquad (7)$$

with $E = [(1 - \nu_{tip}^2)/E_{tip} + (1 - \nu_s^2)/E_s]^{-1}$ where E_{tip}, E_s, ν_{tip}, and ν_s are, respectively, the Young modulus and the Poisson ratio of the tip and the sample. Finally, we obtain the following relationship for N_c^{tot}:

$$N_c^{tot} \cong \frac{A_{av}}{\pi R_c^2} \cong \frac{4r_K R_T(1+KF_N^{2/3})}{R_a^2} \cong \frac{4R_T(1+KF_N^{2/3})}{R_a} \qquad (8)$$

Using eq 3, 4, and 8, we find the following equation for the capillary force as a function of the normal load, humidity, and velocity:

$$F_c \cong 8\pi\gamma R_T(1 + KF_N^{2/3})\left(\frac{V_M}{\lambda R_c^2}\right)\frac{\ln\frac{v_0}{v}}{\ln\frac{P_S}{P}} \qquad (9)$$

Here, we have considered $\theta_T \approx 90$ and $\theta_S \approx 0$, since these are the conditions during our measurements. In this equation we obtain the $^2/_3$ power law dependence of the capillary force on

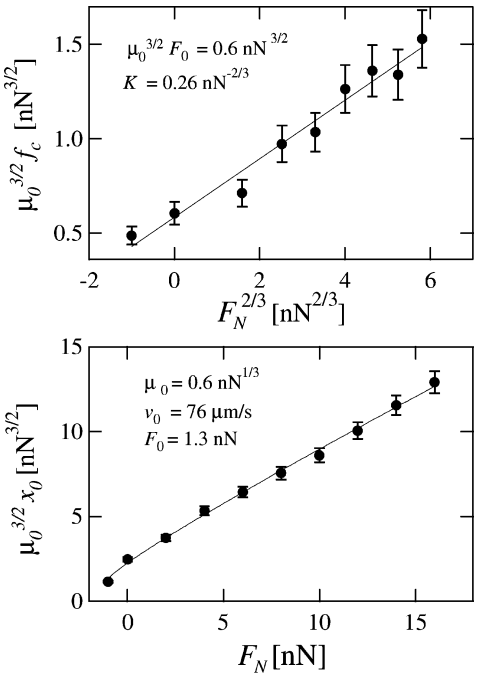

Figure 6. Load dependence of $\mu_0^{3/2}f_c$ and $\mu_0^{3/2}x_0$ obtained by fitting the data in Figure 1 with the equation $F_F = \mu_0(x_0 + f_c \ln v)^{2/3}$.

the load in agreement with the above experiments. Putting eq 9 in eq 6, we obtain

$$F_F \cong \mu_0\left(F_N + F_0(1 + K{F_N}^{2/3})\frac{\ln\frac{v_0}{v}}{\ln\frac{P_S}{P}}\right)^{2/3} \tag{10}$$

with

$$F_0 = \frac{8\pi\gamma R_T V_M}{\lambda {R_c}^2} \tag{11}$$

In the following, we compare eq 10 with the experimental data shown in Figure 1 and with other measurements of the humidity and velocity dependence of friction. With these measurements, the validity of our model is confirmed and we are able to extract important information such as the values of K, v_0, and μ_0. The data in Figure 1 with F_F plotted as a function of ln v for different loads have been fitted with eq 9 rewritten as follows:

$$F_F = \mu_0(x_0 + f_c \ln v[\mu\text{m/s}])^{2/3} \tag{12}$$

with

$$f_c = \left(F_0(1 + K{F_N}^{2/3})\frac{1}{\ln\frac{P_S}{P}}\right) \tag{13}$$

and

$$x_0 = \left(F_N + F_0(1 + K{F_N}^{2/3})\frac{\ln v_0}{\ln\frac{P_S}{P}}\right) \tag{14}$$

The values of $\mu_0^{3/2}f_c$ and $\mu_0^{3/2}x_0$ as a function of the normal load are presented in Figure 6. The linear increase of f_c with $F_N^{2/3}$ confirms the predictions of our model as it is rationalized in eq 13. At higher loads the number of asperities where the capillaries can form is larger, thus the phenomenon of capillary condensation plays a more important role leading to an increased slope of the $F_F(\ln v)$ curves.

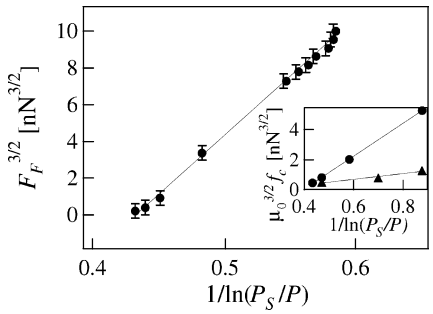

Figure 7. Friction force as a function of the relative humidity for $F_N = 12$ nN and $v = 0.2$ μm/s. The inset shows the humidity dependence of $\mu_0^{3/2}f_c$ for $F_N = 8$ (triangles) and 14 nN (circles).

TABLE 1: Experimental and Theoretical Values of $\mu_0^{3/2}f_c$ for $F_N = 8$ nN

P/P_S	$(\mu_0^{3/2}f_c)_{theor}$ [nN$^{3/2}$]	$(\mu_0^{3/2}f_c)_{exptl}$ [nN$^{3/2}$]
0.12	0.6	0.5 ± 0.1
0.22	0.9	0.8 ± 0.1
0.33	1.3	1.3 ± 0.1

By comparison of the experimental data in Figure 6 with eq 13 and 14, we can determine F_0, K, v_0, and μ_0. To fit $\mu_0^{3/2}f_c$ versus $F_N^{2/3}$ we use two free parameters: $\mu_0^{3/2}F_0$ and K, whereas to fit $\mu_0^{3/2}x_0$ versus F_N we use as free-fitting parameters F_0 and v_0, because K and $\mu_0^{3/2}F_0$ are fixed to the values found in the previous fit. We obtain $F_0 = 1.3 \pm 0.4$ nN which has to be compared with eq 11. From this comparison, by taking $\lambda = 1$ nm and $R_c = 1$ nm we calculate $R_T \approx 30$ nm which is in agreement with our expectations for the tip used during the experiments. Furthermore, our fits give $K = 0.20 \pm 0.15$ nN$^{-2/3}$ which is of the same order of magnitude as the value of 0.02 nN$^{-2/3}$ coming from eq 7 with $E = 40$ GPa, $r_K = 1$ nm, and $R_T = 30$ nm. Finally, the fits give $v_0 = 76$ μm/s and $\mu_0 = 0.6 \pm 0.2$ nN$^{1/3}$.

The humidity dependence of the friction force has been studied at different normal loads and velocities. At $v = 0.2$ μm/s, in the range of relative humidities 4−20%, we show in Figure 7 that F_F grows linearly with $1/\ln(P_S/P)$ as predicted by eq 9. In the inset we show our measurements of $\mu_0^{3/2}f_c$ as a function of $1/\ln(P_S/P)$ at two loads, $F_N = 8$ and 14 nN. As predicted by eq 13, f_c increases linearly with $1/\ln(P_S/P)$ because at higher humidities more capillaries can form at the same sliding velocity. Furthermore, at higher normal loads f_c increases more rapidly with the humidity. Again, this is related to the increase of the efficiency of the capillary condensation process at higher normal loads and confirms the link between humidity and load as described in our model. In Table 1 we show the humidity dependence of $\mu_0^{3/2}f_c$ found directly from measurements of F_F versus ln v at different humidities and found from eq 13 using the values of μ_0, F_0, and K previously obtained from the fit of the data in Figure 1 ($P/P_S = 0.33$) with the equations of our model. The very good agreement between these values definitely proves the correctness of eq 9 in describing the capillary force.

Conclusions

In conclusion, we have found that during the sliding of an AFM tip on a hydrophilic rough surface water capillary bridges can form between the tip and the asperities of the surface. We have shown experimentally and theoretically that the total capillary force due to these bridges increases with the normal

load following a $^2/_3$ power law. We trace back this behavior to the fact that the number of asperities where the water bridges can form increases with $F_N^{2/3}$.

References and Notes

(1) Israelachvili, J. *Intermolecular and Surface Forces*; Academic Press: San Diego, CA, 1997.
(2) Bhushan, B.; Israelachvili, J.; Landman, U. *Nature* **1995**, *374*, 607.
(3) Persson, B. N. J. *Sliding Friction: Physical Principles and Applications*, 2nd ed.; Springer: Berlin, 2000.
(4) Zitzler, L.; Herminghaus, S.; Mugele, F. *Phys. Rev. B* **2002**, *66*, 155436.
(5) Meyer, E.; Overney, R. M.; Dransfeld, K.; Gyalog, T. *Nanoscience: Friction and Rheology on the Nanometer Scale*; World Scientific: Singapore, 1998.
(6) Binggeli, M.; Mate, C. M. *Appl. Phys. Lett.* **1994**, *65*, 415.
(7) Xiao, X.; Qian, L. *Langmuir* **2000**, *16*, 8153.
(8) Gnecco, E.; Bennewitz, R.; Gyalog, T.; Loppacheer, C.; Bammerlin, M.; Meyer, E.; Güntherodt, H. J. *Phys. Rev. Lett.* **2000**, *84*, 1172.
(9) McFarlane, J. S.; Tabor, D. *Proc. R. Soc. (London)* **1950**, *A202*, 224.
(10) Orr, F. M.; Scriven, L. E.; Rivas, A. P. *J. Fluid Mech.* **1975**, *67*, 723.
(11) Fisher, L.; Israelachvili, J. *J. Colloid Interface Sci*. **1981**, *80*, 528.
(12) Kohonen, M. M.; Maeda, N.; Christenson, H. K. *Phys. Rev. Lett*. **1999**, *82*, 4667.
(13) Kim, S.; Christenson, H. K.; Curry, J. E. *J. Phys. Chem. B* **2003**, *107*, 3774.
(14) Jones, R.; Pollock, H.; Cleaver, J.; Hodges, C. S. *Langmuir* **2002**, *18*, 8045.
(15) Liu, H.; Ahmed, S. I.-U.; Scherge, M. *Thin Solid Films* **2001**, *381*, 135.
(16) Riedo, E.; Levy, F.; Brune, H. *Phys. Rev. Lett*. **2002**, *88*, 185505−1.
(17) Bocquet, L.; Charlaix, E.; Ciliberto, S.; Crassous, J. *Nature* **1998**, *396*, 735.
(18) Ando, Y. *Wear* **2000**, *238*, 12.
(19) Halsey, T. C.; Levine, A. L. *Phys. Rev. Lett.* **1998**, *80*, 3141.
(20) Restagno, F.; Crassous, J.; Cottin-Bizonne, C.; Charlaix, E. *Phys. Rev. E* **2002**, *65*, 042301.
(21) Jones, R. *Granular Matter* **2003**, *4*, 191.
(22) Schwarz, U. D.; Zworner, O.; Koster, P.; Wiesendanger, R. *Phys. Rev. B* **1997**, *56*, 6987.
(23) Enachescu, M.; van den Oetelaar, R.; Carpick, R.; Ogletree, D.; Flipse, C.; Salmeron, M. *Phys. Rev. Lett.* **1998**, *81*, 1877.
(24) Fogden, A.; White, L. R. *J. Colloid Interface Sci.* **1990**, *138*, 414.
(25) Bowden, F. P.; Tabor, D. *Friction and Lubrication of Solids: Part I*.; Oxford University Press: 1950.
(26) Johnson, K. L. *Contact Mechanics*; University Press: Cambridge, 1987.
(27) Enachescu, M.; van den Oetelaar, R. J. A.; Carpick R. W.; Ogletree D. F.; Flipse C. F. J.; Salmeron M. *Phys. Rev. Lett.* **1998**, *81*, 1877.
(28) Greenwood, J. A. *Fundamentals of Friction*; Kluwer: Dordrecht, 1992.
(29) Riedo, E.; Brune, H. *Appl. Phys. Lett*. **2003**, *83*, 1986.
(30) Persson, B. N. J. *Phys. Rev. Lett.* **2001**, *87*, 1161.
(31) Riedo, E.; Gnecco, E.; Bennewitz, R.; Meyer, E.; Brune, H. *Phys. Rev. Lett.* **2003**, *91*, 084502.